Chapter

Roles of Cobalt Doping on Structural and Optical of ZnO Thin Films by Ultrasonic Spray Pyrolysis

Sabrina Roguai and Abdelkader Djelloul

Abstract

Here we report a systematic study of structural, optical, and magnetic measurements of $Zn_{1-x}Co_xO$ (x = 0–0.22 at.%) by Ultrasound pyrolysis spray technique. The hexagonal wurtzite structure of our films is confirmed by X-ray diffraction with an average crystallite size estimated in the range of 18–30 nm. For the optical proprieties, using the Levenberg–Marquardt least squares rule, the experimental transmission measurements were perfectly adapted to the transmission data calculated by a combination of the Wemple-DiDomenico model, the absorption coefficient of an electronic transition and the Tauc-Urbach model. The concentration of the NCo absorption centers and the oscillator intensity f of the d-d transition of Co2+ ions are determined by the Smakula method. The presence of high concentrations of localized states in the thin films is responsible for the reduction in the width of optical bandgap.

Keywords: thin films, X-ray diffraction, optical properties

1. Introduction

Zinc oxide is a transparent direct gap and wide band gap semiconductor (3.37 eV) with a fairly high excitonic binding energy of 60 meV at room temperature, it is attracting more and more attention from researchers because of its wide range applications, in particular in the field of spintronics [1–4]. Zinc oxide is a transparent material with a transmission value of 0.9 in the visible, crystallizes in a wurtzite-like structure defined by a hexagonal lattice where zinc ions occupy the centers of the tetrahedral sites and oxygen ions occupy the vertices.

The improvement of the properties of thin ZnO layers is commonly achieved through doping. Among the different dopants, cobalt (Co) thanks to the similarity between the ionic rays (r_{Co2+} = 0.058 nm) and (r_{Zn2+} = 0.060 nm). In order to obtain what is called Diluted Magnetic Semi-conductor (DMS), these DMS play an important role as they allow the integration of certain components of spintronics and optoelectronics [5–10].

Different technological processes can be used to deposit cobalt-doped ZnO in thin films [11–14]. The doping of ZnO with transition metal ions such as Co (substitution of Zn + 2 ions by Co + 2 ions) induces magnetic properties due to its

possible applications in the field of spintronics. Moreover, the excellent optical properties of ZnO and the engineering possibility of the bandgap by doping the matrix with Co2+ ions strongly encourages the exploration of the magneto-optical properties of the Co2+ doped ZnO system [15–17]. Much research work is focused on the elaboration of single-phase Zn1-xCoxO thin films with several techniques [18].

The determination of the optical constants (refractive index, extinction coefficient, thickness) of thin films is of great interest both on a fundamental and technological level. Among the various techniques commonly used to deduce these parameters, we can cite the techniques of optical transmission, X-ray reflectometry and ellipsometry.

ZnO thin films, depending on the cobalt doping concentration, have a high transparency of more than 90% in the visible (400–750 nm) and infrared range. Three absorption bands located at 568, 608 and 659 nm that can be attributed to the dd transitions of the tetrahedrally coordinated Co2+ ion in the high spin state are attributed respectively: A_2 4 (F) → A_1 (G) $_2$, A_2 4 (F) → T_1 (P) $_4$ and A_2 4 (F) → E (G) $_2$. The value of *Eg* for the ZnO thin film was found to be increased from 3.26 eV to 3.31 eV with an increase in the Co doping concentration. The increase of the bandgap can be attributed to the strong sp-d exchange interaction between the band electrons and the localized d-electrons of the dopant [19].

In this study, thin layers of ZnO, $Zn_{1-x}Co_xO$ deposited by the ultason pyrolysis spray technique at a temperature of 450 °C weighing 30 min.. and their structural and optical properties are reported in this work. A particular attention is given to the theoretical methods used for the determination of the dispersion parameters of the films using only a single transmission spectrum.

2. Experimental

2.1 Film preparation

ZnO, $Zn_{1-x}Co_xO$ thin films have been developed by the pyrolysis spray technique, is well known for its simplicity and possibility to produce large area films. The properties of the deposited material can be changed and controlled by appropriate optimization of the deposition conditions, on glass substrates (solid glass), the choice of glass as the deposition substrate was adopted because of the good thermal expansion it presents with ZnO ($\alpha_{verre} = 8.5.10^{-6}\ K^{-1}$, $\alpha_{ZnO} = 7.2.10^{-6}\ K^{-1}$) so as to minimize the stresses at the substrate layer interface, and for economic reasons, for their transparency which is well suited for the optical characterization of films in the visible.

We used, in this work, 0.01 M of zinc acetate [$Zn(CH_3COO)_2.2H_2O$)] (Fulka 99.9%);comme matériau source (de ZnO) que nous avons dissous dans 50 ml deionized water (resistivity = 18.2 MΩ.cm); 20 ml CH_3OH (Merck 99.5%); 30 ml C_2H_5OH (Merck 99.5%) and Cobalt nitrate hexahydrate 1–22% (Co, at. %) [Co $(NO_3)_2{\cdot}6H_2O$] has been used as the Co source. A small amount of acetic acid was added to the aqueous solution for adjusting the pH value to about 4.8, in order to prevent the formation of hydroxides. Further details are reported elsewhere [20].

The structural properties of the thin films were studied by an X-ray diffractometer Rigaku Ultima IV powder equipped with CuKα radiation (λ = 1.54 Å). X-ray diffraction (XRD) data were recorded at a scanning speed of 2 degree/min, between 20° and 80°. The optical properties of the films were studied by recording the transmittance spectra of the films within the wavelength range of 190–1800 nm using a Perkin Elmer UV–VIS–NIR Lambda 19 spectrophotometer.

3. Results and discussion

3.1 Structure and microstructure analysis

Figure 1 shows the DRX diagram of a thin layer of cobalt doped ZnO. It can be seen from the spectrum that the films are well crystallized. The different diffraction peaks correspond to the (100), (002), (101), (102), (110), (103), (112) planes of hexagonal wurtzite structure of polycrystalline ZnO (Card. JCPDS N0 36–1451), and no other crystalline phase was detected. Peak intensities vary considerably depending on the Co. The preferred direction of growth during deposition changes with the level of Co doping: along (002) for pure ZnO, (101) for xCo = 0.01, then again (002) for xCo in the range of 0.03–0.14, and finally at varying orientations for even higher Co content.

Table 1 illustrates the various results of X-ray diffraction Rietveld refinements results. It can be noticed that the size of crystallite varies within a narrow interval of 18–30 nm, whereas the micro-strain changes considerably with Co content in to the range of 0.131–0.289%.

The evolution of the mesh parameter a and c of the Zn1-xCoxO thin films as a function of the doping rate is shown in **Table 1**. Indeed, the mesh parameters were calculated using the Bragg's law and from the peak (002) of the X-ray diffractogram. An increase of the a mesh parameter is noted while the c parameter was not affected, accompanied with an increase of the unit volume when the cobalt level increases. However, the development of network parameters with a Co rate is more difficult than expected. Four points must be taken as a reference, as their effects occur concomitantly:

1. According to Vegard's law, the lattice parameters are expected to decrease slightly as the Co level increases, the ionic radius of Co is smaller than that of Zn. In fact, in our case, the ionic radius of Co is slightly smaller than that of Zn^{2+} in tetrahedral coordination with an ionic radius of 0.060 nm will not be completely filled by Co^{2+} in tetrahedral coordination with an (r_{Co2+} = 0.058 nm) but also with Co^{2+} in octahedral coordination with an r = 0.065 nm (low spin) or/and 0.075 nm (high spin) [21]. The substitution of Co into tetrahedral coordination was confirmed by transmittance measurements (see section 3.2).

2. Depending on the size impact in the nanomaterials, the lattice contraction is assumed to occur when the particle size (crystallites) reduces [22].

3. The mismatch between the glass substrate and the thin film (ZnO) deposited causes a certain constraint in the ZnO and may cause some distortion of the lattice, so that the lattice parameters may vary depending on this [23].

4. Influence of the deposition temperature (450 °C) on the stoichiometry, which means that possible gaps in O and/or Zn are likely to be created, and that O can even fill interstitial sites [24]. This will lead to anisotropic changes in the properties of the matrix.

5. Several Zn or/and Co could also invest interstitial sites, which would cause a disturbance of the layout parameters of the lattice.

3.2 Optical properties

The refractive index (n) is very important in the determination of the optical properties of semiconductors. Knowledge of the refractive index is essential in the

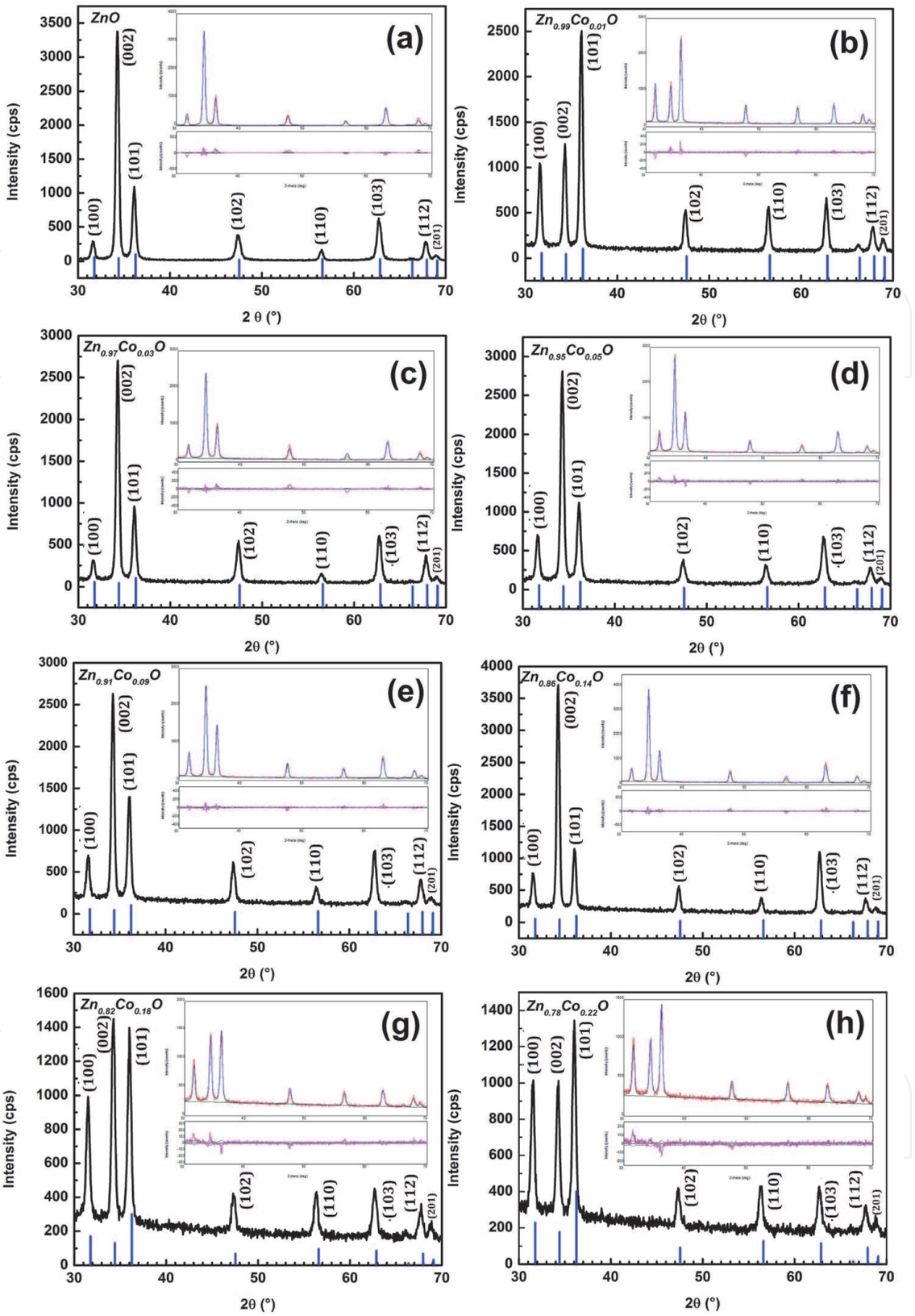

Figure 1.
XRD patterns of (a) pure ZnO film and (b–h) Co-doped $Zn_{1-x}Co_xO$ thin films. The XRD (b–h) correspond to the Co atomic content of 1%, 3%, 5%, 9%, 14%, 18% and 22%, respectively. The inset shows the Rietveld refinements of $Zn_{1-x}Co_xO$ composition. Solid blue curve: Calculated pattern; red solid line: Experimental data; solid orange line (down): Intensity difference.

design of laser heterostructures, optoelectronic devices, and solar cell applications. From the transmission spectra obtained for the ZnO, Zn1-xCoxO layers, the refractive index can be determined. The refractive index of the film can be calculated using a single-effective-oscillator fit, proposed by Wemple et al. [25], of the form

Composition	Crystallite Size (nm)	Microstrain (%)	Lattice Parameters (Å)	R_{wp}(%)	Refinements R_p (%)	Factors R_e (%)	S	χ^2
ZnO	25	0.266	*a* = 3.2542 *c* = 5.2129	16.87	11.84	8.93	1.71	2.92
$Zn_{0.99}Co_{0.01}O$	21	0.096	*a* = 3.2577 *c* = 5.2124	9.21	7.37	7.55	1.21	1.48
$Zn_{0.97}Co_{0.03}O$	35	0.230	*a* = 3.2594 *c* = 5.2172	8.23	6.28	5.40	1.52	2.32
$Zn_{0.95}Co_{0.05}O$	23	0.289	*a* = 3.2572 *c* = 5.2162	9.58	7.41	7.63	1.25	1.57
$Zn_{0.91}Co_{0.09}O$	22	0.131	*a* = 3.2613 *c* = 5.2172	8.55	6.64	6.76	1.26	1.59
$Zn_{0.86}Co_{0.14}O$	25	0.143	*a* = 3.2605 *c* = 5.2148	8.94	6.99	6.15	1.45	2.11
$Zn_{0.82}Co_{0.18}O$	18	0.147	*a* = 3.2689 *c* = 5.2230	8.40	6.72	6.18	1.36	1.85
$Zn_{0.78}Co_{0.22}O$	18	0.142	*a* = 3.2644 *c* = 5.2167	8.02	6.55	6.12	1.31	1.71

Table 1.
X-ray diffraction Rietveld refinements results.

$n^2 - 1 = E_d E_0 / \left(E_0^2 - E^2\right)$ where $E = hc/\lambda$ is the photon energy, E_0 the single oscillator energy, and E_d is the dispersion energy. The parameter E_d, which is a measure of the strength of inter-band optical transitions, is found to obey the simple empirical relationship $E_d = \beta N_C Z_a N_e$ in which NC is the coordination number of the cation closest to the anion, Za is the formal chemical valence of the anion, Ne is the effective number of valence electrons per anion (usually Ne = 8), and for the ionic βi = 0.26 ± 0.04 eV. The values of E0, Ed and β of ZnO are listed in **Table 2**.

Information on the dispersion of the refractive index below the band gap can be evaluated by the dispersion correlation below:

$$n^2 - 1 = \frac{S_0 \lambda_0^2}{1 - (\lambda_0/\lambda)^2} \tag{1}$$

in which λ is the wavelength of the incident light, S0 is the average oscillator power of the absorption band with the resonance wavelength λ0, which is an average oscillator wavelength. The equation Eq. (1) is also transformed into:

$$n^2 - 1 = \frac{\left(n_\infty^2 - 1\right)\lambda^2}{\lambda^2 - \lambda_0^2} \tag{2}$$

where n_∞ and λ_0 are the high-frequency refractive index and average oscillator wavelength, respectively.

When absorption bands in the visible and near infrared regions coexist (extinction coefficient, $k \neq 0$), the refractive index dispersion data can be analyzed by the following dispersion relation:

$$n^2 - 1 - k^2 = \frac{\left(n_\infty^2 - 1\right)\lambda^2}{\lambda^2 - \lambda_0^2} \tag{3}$$

Cristal	E_0 (eV)	E_d (eV)	M_{-1}	M_{-3}, 10^{-2} $(eV)^{-2}$	n_∞	n at 598 nm	β (eV)
ZnO	6.4	17.1	2.672	6.523	1.916	1.996	0.27

Table 2.
Dispersion parameters for ZnO [34]. Wurtzite (N_C = 4, Z_a = 2, N_e = 8).

In cases where the absorption of a chemical system shows the "simple form" band of absorption, the electronic transition is capable of correctly representing the same band. To replicate the structure of this absorption band, a simple Gaussian profile centred on the vertical transition in question is then used. This assumes a vertical electronic transition between the state Si and the state Sj, the wavelength o electron transition $\lambda_{i\rightarrow j}$ and the strength of the oscillator $f_{i\rightarrow j}$ The resulting spectral band's expression $\alpha_{i\rightarrow j}$ is proportional to a Gaussian function such as:

$$\alpha_{i\rightarrow j}(\lambda)\propto\frac{f_{i\rightarrow j}}{\xi'\sqrt{\pi}}\exp\left(-\frac{\left(\lambda-\lambda_{i\rightarrow j}\right)^2}{\xi'^2}\right),\xi'=\frac{\xi}{2\sqrt{\ln(2)}} \tag{4}$$

where ξ represents the width at half maximum of the Gaussian function, or bandwidth. This parameter is chosen empirically by comparison with experiment.

In a simple solid consisting of a host lattice and an impurity ion, the absorption coefficient α for the solid solution can be considered as the sum $\alpha = \alpha_h + \alpha_i$, where α_h, is the absorption from the host lattice and α_i is the contribution to the absorption coefficient from the impurity ion.

Whereξ the distance at the half limit of the Gaussian function or bandwidth is represented. Compared to experiments, this parameter is selected empirically.

The absorption coefficient α for the solid solution can be considered as the sum $\alpha = \alpha_h + \alpha_i$, I where α_h, is the absorption from the host lattice and α_I is the contribution to the absorption coefficient from the impurity ion, in a simple solid consisting of a host lattice and an impurity ion.

α_h is equal to the absorption coefficient for the un-doped ZnO for ZnO:Co.

The extinction coefficient k is related by the expression $4\pi k/\lambda$ to the absorption coefficient α. In the transparent range ($\lambda \geq \lambda_g$), the extinction coefficient k is [29]:

$$k=k_0\frac{\left(\exp\left(B\lambda_g/\lambda\right)-1\right)}{\left(\exp\left(B\right)-1\right)}+\frac{\lambda}{4\pi}\left[\alpha_0+\sum_{j=1}^{q}\alpha_{i\rightarrow j}(\lambda)\right] \tag{5}$$

where λ_g - wavelength of absorption region ($E_g(eV)=1239.8/\lambda_g(nm)$), i - ground state, j - excited state and q is the number of excited states.

The extinction coefficient k in the region of interband transitions ($\lambda \leq \lambda_g$) is:

$$k=k_1\left(1-\frac{\lambda}{\lambda_g}\right)^r+k_0 \tag{6}$$

In which k_0, k_1, B, λ_g, $f_{i\rightarrow j}$, ξ' and $\lambda_{i\rightarrow j}$ are the fitting parameters, r can, depending on the nature of the interband electronic transitions, have values such as 1/2, 3/2, 2, and 3, such as direct permitted, direct prohibited, indirect permitted and indirect prohibited transitions, respectively [26, 27]. The value of r for ZnO is always 1/2, i.e. the fundamental absorption corresponds to the direct transformation permitted.

Formulas relating the measured values of T(λ) and thickness, d, to the real and imaginary components of the refractive index, N = *n-ik*, for the absorbing film on a

transparent substrate are necessary for the measurement of the optical constants from the data. The common approach is to consider light reflection and transmission at the three interfaces of the multilayer structure of the air/film/substrate/air and to express the results in terms of Fresnel coefficients.

The device is encircled by air with a refractive index of $n_0 = 1$. Taking into account all the multiple reflections at the three interfaces, it can be seen that the expression of the transmittance T(λ) for normal incidence is given in the case where $k^2 << n^2$ is given in [20]:

$$T = \frac{A\chi}{B - C\chi + D\chi^2} \tag{7}$$

where,

$$A = 16\gamma^2 n_s\left(n^2 + k^2\right)$$

$$B = \left[(n+1)^2 + k^2\right]\left[(n+1)\left(n + n_S^2\right) + k^2\right]$$

$$C = 2\eta\left[\left(n^2 - 1 + k^2\right)\left(n^2 - n_S^2 + k^2\right) - 2k^2\left(n_S^2 + 1\right)\right]\cos\varphi - 2k\eta\left[2\left(n^2 - n_S^2 + k^2\right) + \left(n_S^2 + 1\right)\left(n^2 - 1 + k^2\right)\right]\sin\varphi D = \eta^2\left[(n-1)^2 + k^2\right]\left[(n-1)\left(n - n_S^2\right) + k^2\right]$$

$$\varphi = 4\pi n d/\lambda$$

$$\chi = \exp\left(-\alpha d\right)$$

$$\alpha = 4\pi k/\lambda$$

$$\gamma = \exp\left[-\tfrac{1}{2}(2\pi\sigma/\lambda)^2(1-n)^2\right], \eta = \exp\left[-2(2\pi\sigma/\lambda)^2\right].$$

When σ is the height of surface irregularity for rms. The parameters n and k are the real and imaginary components of the refractive index of the thin film, d is the thickness of the film and ns is the refractive index of the real substratum. Knowing the substrate's refractive index and putting the n and k values as calculated from Eqs. (3), in Eqs. (5) and (6) respectively, in Eq. (7), it is possible to obtain the theoretical transmittance value, referred to as T_{Theo}. Then the experimental transmittance data (T_{expt}) was completely fitted with the transmittance data measured (T_{theo}) by Eq. (7) by the application of the Levenberg–Marquardt least square method, through a combination of the Wemple-DiDomenico model, the electronic transition absorption coefficient, and the Tauc-Urbach model.

The exact film thickness and energy bandgap can be determined by minimizing the sum of squares ($|T_{expt}\text{-}T_{theo}|$) created for different values of thickness (d) and gap wavelength (λg) by iterative technique and finding the corresponding n and k.

The glass substrate refractive index, taken from Ref. [28], is:

$$n_S^2 = 1 + \frac{1.0396 \times \lambda^2}{\lambda^2 - 6.0069 \times 10^3} + \frac{0.23179 \times \lambda^2}{\lambda^2 - 2.0017 \times 10^4} + \frac{1.0104 \times \lambda^2}{\lambda^2 - 1.0356 \times 10^8} \tag{8}$$

Transmittance spectra were taken at room temperature to study the optical properties of $Zn_{1-x}Co_xO$ films. At wavelengths of 565, 611, 657, 1297, 1410 and 1648 nm, the transmittance spectra of all films display the characteristic Co^{2+} absorption in the visible and near infrared spectral area. The prevalent absorption is the first three peaks.

The colorless host lattice (ZnO) is converted into green by the dopant (Co^{2+}) ionIf the concentration of dopant ions is low, it is possible to ignore the interaction between the dopant ions. This is what has been perceived as an isolated center of absorption here. In the studied systems, the actual distance between two Zn atoms is around ~0.326 nm, while the Zn atoms in $Zn_{1-x}Co_xO$ are present with ZnO distances of 0.196 nm in tetrahedral structures. The mean distance between Co ions that have been replaced by Zn sites within the ZnO crystal lattice can be calculated

for uniformly distributed Co ions through [29] $N_{at} = (4/3)\ (Z/V_C)\ \pi\ r^3$, where r is the average radius of an atomic sphere and Nat is the number of atoms in the sphere. The structural parameters for $Zn_{0.95}Co_{0.05}O$ are: a = 0.32572 nm, c = 0.52162 nm; volume of unit cell (V_C) = 47.92×10^{-3} nm^3; Z = 2. For zinc atoms in a wurtzite structure of $Zn_{0.95}Co_{0.05}O$, $Z/V_C = 41.73\ nm^{-3}$. Co ion occupy 5% of the zinc sites in the $Zn_{0.95}Co_{0.05}O$film. The 20th position of zinc from the probe atom is also occupied by cobalt. The average distance between Co ions is calculated to be about ~0.48 nm using the above measurement, indicating that the closest Co ion to a Co ion probe is located in the next unit cell.

According to the ligand field theory [20], splitting of $3d^7$ (Co^{2+}) orbital should result in the spectroscopic terms $^4A_2$ (*A*: no degeneracy), $^4T_2$, $^4T_1$ (*T*: three fold degeneracy), and ^2E (*E*: two fold degeneracy). For Co^{2+} in ZnO crystal lattice, Co^{2+} substitutes for some Zn^{2+}, and adopts tetrahedral ligand coordination. The 3d levels are extremely host sensitive. The strong crystal field in ZnO leads to the splitting of 3d electron orbits of Co^{2+} and produces the ground level: $^4A_2$, and the excited states: ^2E, $^4T_2$, and $^4T_1$, etc. The transitions from $^4A_2$ to $^4T_2$, and $^4T_1$ are spin-allowed.

Figures 2 and **3** show UV spectra of ZnO and $Zn_{1-x}Co_xO$ films. The absorption peaks located at 657, 610, and 567 nm for $Zn_{1-x}Co_xO$ films can be assigned as $^4A_2(F) \rightarrow {}^2E(G)$, $^4A_2(F) \rightarrow {}^4T_1(P)$, and $^4A_2(F) \rightarrow {}^2A_1\ (G)$, of Co^{2+}, attributed to the crystal field transitions in the high spin state of Co^{2+} in the tetrahedral coordination, suggesting that the tetrahedrally coordinated Co^{2+} ions substitute for Zn^{2+} ions in the hexagonal ZnO wurtzite structure [20]. Between 1272 and 1647 nm, additional crystal field transition was observed, namely $^4A_2(F) \rightarrow {}^4T_1(F)$ transition.

In **Figures 2** and **3**, the strong curve, refer to the fitting of the curve using Eq. (7) and the symbol represents the data from the experiments. The figures indicate a fair fit for the experimental results, indicating the precise determination of the parameters of Eq. (7). **Table 3** presents the values of d, Eg, Ed, E0, rms and n, derived by fitting the experimental data with Eq. (7).

The pure ZnO film optical energy band-gap was measured to be 3.26 eV. This value is marginally lower than the bulk value of 3.31 eV [1], and is in good alignment with the ZnO thin film data previously reported [30].

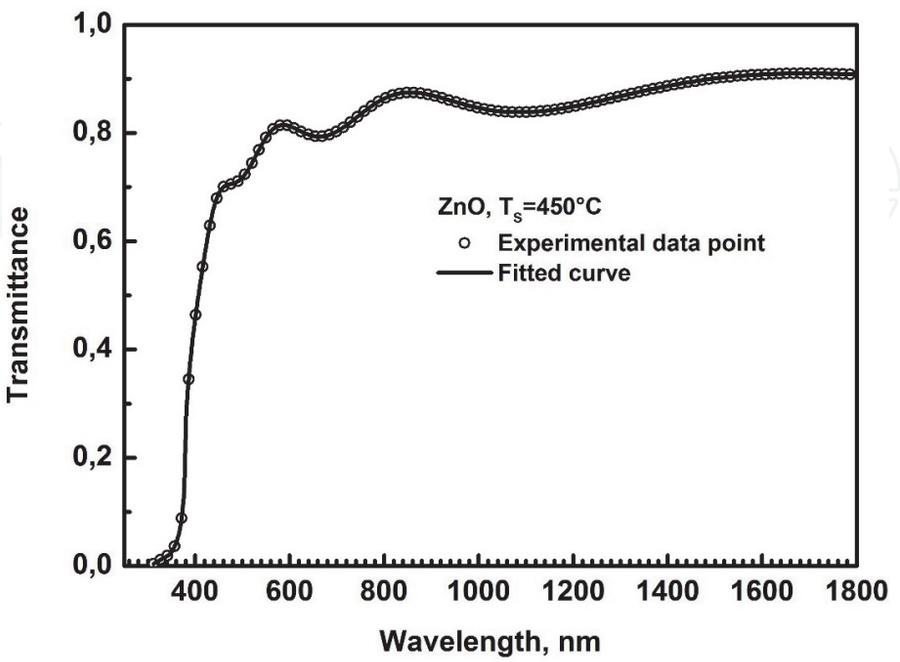

Figure 2.
Transmission spectrum of ZnO films deposited on glass substrate at 450 °C is presented as a reference. Measured (full circles) and calculated (solid lines) transmittance spectra of films.

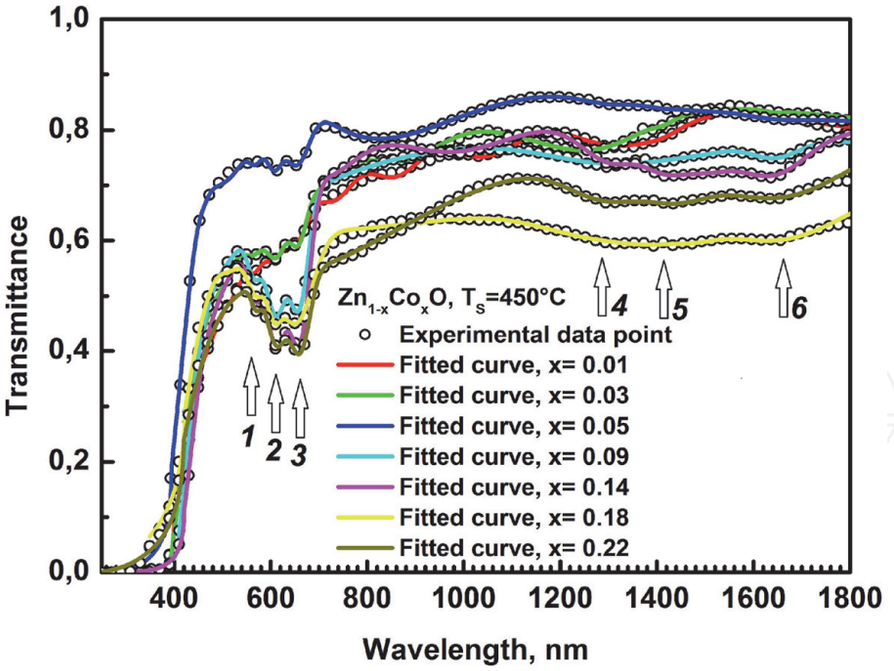

Figure 3.
Transmission spectra of $Zn_{1-x}Co_xO$ films deposited on glass substrate at 450 °C. measured (full circles) and calculated (solid lines) transmittance spectra of films.

The direct optical bandgap value will be reduced from 3.26 to 3.00 eV. The interactions of s-d and p-dexchange lead to a negative and positive correction of the conduction band and the edges of the valence band, resulting in the narrowing of the band gap. The interaction results in energy band corrections; the conduction band is lowered while the valence band is increased, causing the band gap to decrease [20].

The decrease in energy value from 3.26 eV (pure ZnO) to 3.00 eV ($Zn_{0.78}Co_{0.22}O$) appears to be due to active transitions involving 3d Co^{2+} ion levels and intense sp–d interactions between the itinerant 'sp' carriers (band electrons) and the dopant's localized 'd' electrons. Several researchers have already recorded this red change of band-gap Eg with the incorporation of Co^{2+} into ZnO [31].

Using single oscillator energy (E_0) and dispersion energy (E_d) obtained from the fitted transmittance spectra reported in **Table 3**, M_{-1} and M_{-3} moments of the optical spectra can be determined from the following two Equations [25]:

	Thickness, nm	E_g, eV	E_d, eV	E_0, eV	*n* at 598 nm	n_∞	M_{-1}	M_{-3}, $\times 10^{-2}$ $(eV)^{-2}$	σ, nm	Porosity %
ZnO	486	3.258	11.334	6.018	1.771	1.698	1.883	5.200	38	17.0
$Zn_{0.99}Co_{0.01}O$	1350	3.177	12.373	6.198	1.802	1.731	1.996	5.196	128	14.1
$Zn_{0.97}Co_{0.03}O$	846	3.097	13.478	6.185	1.859	1.783	2.179	5.696	130	09.7
$Zn_{0.95}Co_{0.05}O$	421	3.050	13.422	5.635	1.940	1.839	2.382	7.501	95	03.8
$Zn_{0.91}Co_{0.09}O$	463	3.075	11.621	6.061	1.781	1.708	1.917	5.219	40	15.7
$Zn_{0.86}Co_{0.14}O$	722	2.993	11.872	6.192	1.778	1.708	1.917	5.000	96	16.0
$Zn_{0.82}Co_{0.18}O$	396	3.023	19.290	5.947	2.166	2.060	3.243	9.171	74	/
$Zn_{0.78}Co_{0.22}O$	395	3.009	19.706	6.037	2.169	2.065	3.264	8.956	78	/

Table 3.
Dispersion parameters of the films extracted by fitting the experimental data with Eq.(7).

$$E_0^2 = \frac{M_{-1}}{M_{-3}} \tag{9}$$

$$E_d^2 = \frac{M_{-1}^3}{M_{-3}} \tag{10}$$

These moments represent the measure of the average bond strength. The two moments M_{-1} and M_{-3} were calculated from the data of E_0 and E_d and are given in **Table 3**.

The calculated refractive indices of ZnO and $Zn_{1-x}Co_xO$ films (**Figure 4**) exhibit a function of the wavelength. It is found that the refractive indices at 598 nm of ZnO, $Zn_{0.95}Co_{0.05}O$ and $Zn_{0.78}Co_{0.22}O$ films are equal to 1.77, 1.96 and 2.16, respectively.

It can be noticed that the above calculated refractive indices are equal or a little greater than that of ZnO film prepared under the same conditions. This might be due to the fact that the index of refraction is sensitive to structural defects (for example voids, dopants, inclusions), thus it can provide an important information concerning the microstructure of the material.

It can be observed that the refractive indices measured above are equal to, or slightly greater than, the ZnO film prepared under the same conditions. This may be due to the fact that the refractive index is vulnerable to structural defects (such as voids, dopants, inclusions), so it can provide valuable details about the material's microstructure. As Zn(CH3COO)2 was oxidized into ZnO, gases like CH3COOH, H2O, etc. were manufactured. Consequently, because of the release of these gases, pores can be easily formed. Using the LorentzLorenz Equation [32], porosity P is determined from optical constants:

$$P = 1 - \frac{\left(n_{film}^2 - 1\right)\left(n_{bulk}^2 + 2\right)}{\left(n_{film}^2 + 2\right)\left(n_{bulk}^2 - 1\right)} \tag{11}$$

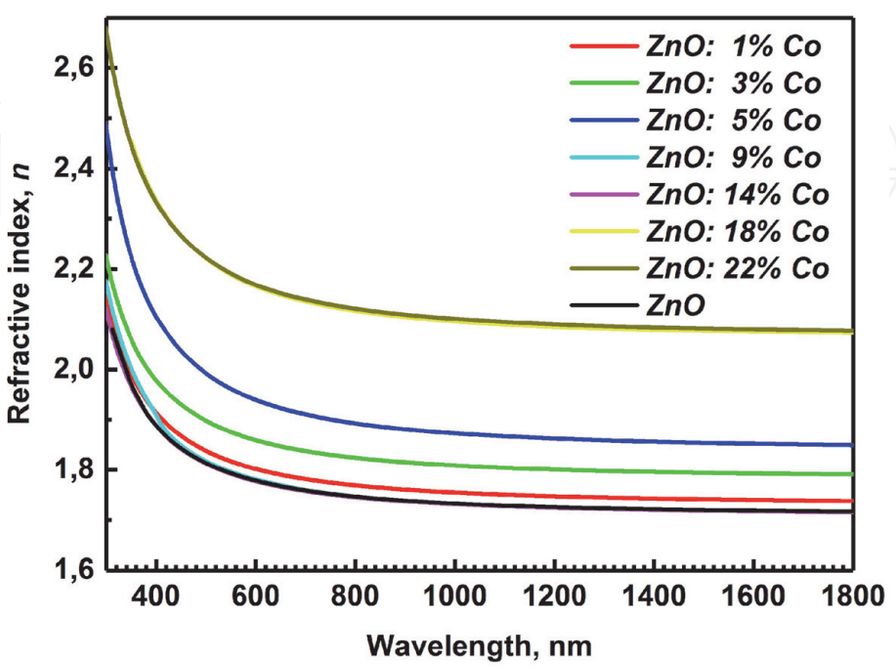

Figure 4.
Refractive index of $Zn_{1-x}Co_xO$ films grown on glass substrate at T_S = 450 °C.

In which the n_{film} value (1,771 at 598 nm) represents the refractive indices of porous ZnO films, the nbulk represents the ZnO bulk refractive indices at the same wavelength of 1,996. The average mass density of the film ρ_{film} is related to the porosity (P) and bulk density (ρ_{bulk}) of ZnO through Eq. (12):

$$\rho_{film} = \rho_{bulk}(1 - P) \tag{12}$$

Against the bulk density ρ_{bulk} = 5.61 g.cm^{-3}, we calculated P = 0.1659 and ρ_{film} = 4.68 g.cm^{-3}. The concentration of cobalt cations N_{Co} for x at. doping level in the films can be measured as:

$$N_{Co} = \frac{\rho_{film} N_{Av}}{M} \times x \tag{13}$$

where N_{Av} is the Avogadro constant and M the molar mass. With the values ρ_{film} = 4.68 g cm^{-3}, N_{Av} = 6.022 × 10^{23} mol^{-1}, and molar mass for ZnO, M = 81.408 g.mol^{-1}, an example (x = 0.05) of the calculated value (x = 0.05) of N_{Co} is 1.73 × 10^{21} cm^{-3}.

As a tool for calculating the concentration of impurities in a host from known values and calculated absorption coefficients, oscillator intensity is also used. Classically, the power of the oscillator f is the number of electric dipole oscillators that can be simulated (inthe dielectric dipole approximation) by the radiation field and has a value close to one for strongly permitted transitions. Integrated optical transition absorption is connected by the well known Smakula formula [33] to the concentration of absorbing centers N, refraction index n, and oscillator intensity f:

$$Nf = 8.21 \times 10^{16} cm^{-3} \frac{n}{(n^2 + 2)^2} \int \alpha(E)\, dE \tag{14}$$

where n is the refractive index of intersubband transitions, α is the decadic absorption coefficient in cm^{-1} and E is the energy in eV. For Gaussian absorption bands the integral is:

$$\frac{1}{2}\sqrt{\frac{\pi}{\ln 2}}\alpha_{\max} W \tag{15}$$

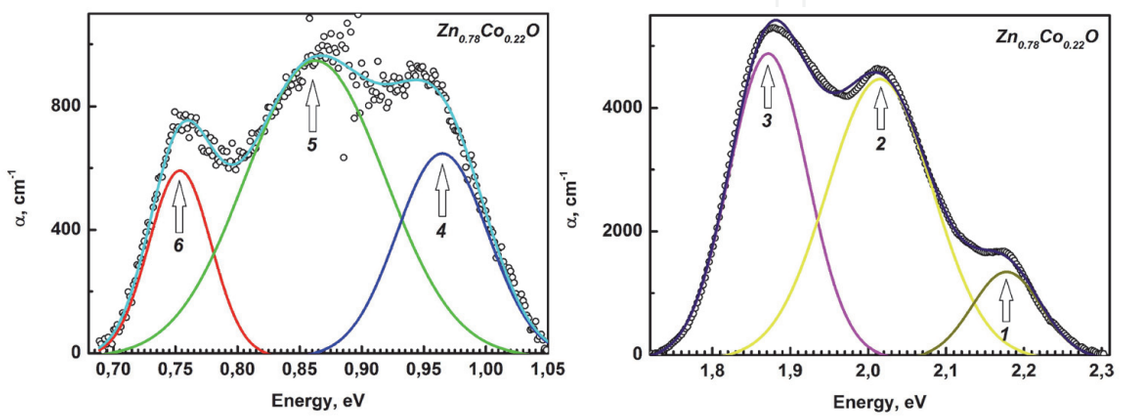

Figure 5.
The Gaussian deconvolution of the absorption coefficient of $Zn_{0.78}Co_{0.22}O$ films deposited on glass substrate at 450 °C.

N° Peak	E_c (eV)	w (eV)	A (eV/cm)	sigma	FWHM (eV)	height (cm^{-1})
1	$2.17774 \pm 6.04092 \times 10^{4}$	0.08866 ± 0.00118	156.38794 ± 3.46173	0.04433	0.10439	1407.38652
2	$2.01508 \pm 3.94746 \times 10^{-4}$	0.13482 ± 0.00125	765.61193 ± 6.88833	0.06741	0.15874	4530.94569
3	$1.87161 \pm 3.34026 \times 10^{-4}$	$0.10097 \pm 4.8835 \times 10^{-4}$	625.04657 ± 6.30209	0.05048	0.11888	4939.46937
4	0.96495 ± 0.00109	0.07376 ± 0.00166	60.94398 ± 3.91289	0.03688	0.08684	659.27169
5	0.86261 ± 0.00123	0.11265 ± 0.00363	135.47616 ± 4.41433	0.05633	0.13264	959.54823
6	$0.75363 \pm 3.62511 \times 10^{-4}$	0.05038 ± 0.00103	38.10798 ± 1.62028	0.02519	0.05932	603.52364

Table 4.
Deconvolution results of the absorption coefficient of the $Zn_{0.78}Co_{0.22}O$ $\alpha(cm^{-1}) \infty \frac{A}{w\sqrt{\pi/2}} \exp\left(-2\left(\frac{E-E_c}{w}\right)^2\right)$ sample by the function.

with maximum absorption α and full width at half maximum W. Eq. (14) can be expressed as follow:

$$Nf = 8.74 \times 10^{16} cm^{-3} \frac{n}{(n^2+2)^2} \alpha_{\max} W \tag{16}$$

Due to the Co^{2+} d-d transitions, it is difficult to measure the absorbance because the total transmittance value is different for each film. The absorption coefficient ($\alpha \approx (1/d) \times \ln(1/T)$) was then used because it is normalized by the thickness of the

	1	2	3	4	5	6
$Zn_{0.99}Co_{0.01}O$: d = 1350 nm, N_{Co}^{cal} = 3.403 × 10^{20} cm^{-3}, N_{Co}^{exp} = 3.622 × 10^{21} cm^{-3}, $\Sigma f_{i \to j}$ = 6.060 × 10^{-3}						
Refractive index	**1.811**	**1.799**	**1.789**	**1.745**	**1.742**	**1.739**
$f_{i \to j}$, ×10^{-3}	**0.161**	**1.472**	**1.452**	**1.481**	**1.481**	**0.010**
N, ×10^{20} cm^{-3}	**11.16**	**1.133**	**3.069**	**1.806**	**0.746**	**18.310**
$Zn_{0.97}Co_{0.03}O$: d = 846 nm, N_{Co}^{cal} = 9.835 × 10^{20} cm^{-3}, N_{Co}^{exp} = 1.223 × 10^{21} cm^{-3}, $\Sigma f_{i \to j}$ = 0.025						
Refractive index	**1.869**	**1.856**	**1.845**	**1.798**	**1.795**	**1.792**
$f_{i \to j}$, ×10^{-3}	**0.597**	**5.803**	**4.696**	**6.934**	**5.998**	**1.039**
N, ×10^{20} cm^{-3}	**6.514**	**1.533**	**2.506**	**1.431**	**0.046**	**0.205**
$Zn_{0.95}Co_{0.05}O$: d = 421 nm, N_{Co}^{cal} = 1.867 × 10^{21} cm^{-3}, N_{Co}^{exp} = 1.393 × 10^{20} cm^{-3}, $\Sigma f_{i \to j}$ = 0.100						
Refractive index	**1.953**	**1.935**	**1.921**	**1.858**	**1.855**	**1.851**
$f_{i \to j}$, ×10^{-3}	**9.665**	**19.88**	**19.48**	**22.11**	**22.31**	**7.224**
N, ×10^{19} cm^{-3}	**2.531**	**5.545**	**4.429**	**0.209**	**0.383**	**0.835**
$Zn_{0.91}Co_{0.09}O$: d = 463 nm, N_{Co}^{cal} = 2.876 × 10^{21} cm^{-3}, N_{Co}^{exp} = 4.887 × 10^{20} cm^{-3}, $\Sigma f_{i \to j}$ = 0.178						
Refractive index	**1.791**	**1.778**	**1.768**	**1.722**	**1.720**	**1.717**
$f_{i \to j}$, ×10^{-3}	**15.10**	**38.86**	**38.87**	**38.45**	**38.87**	**8.333**
N, ×10^{20} cm^{-3}	**1.533**	**1.530**	**1.290**	**0.214**	**0.065**	**0.255**
$Zn_{0.86}Co_{0.14}O$: d = 722 nm, N_{Co}^{cal} = 4.706 × 10^{21} cm^{-3}, N_{Co}^{exp} = 6.307 × 10^{20} cm^{-3}, $\Sigma f_{i \to j}$ = 0.174						
Refractive index	**1.786**	**1.775**	**1.765**	**1.722**	**1.720**	**1.717**
$f_{i \to j}$, ×10^{-3}	**6.730**	**29.53**	**31.38**	**36.31**	**38.78**	**31.206**
N, ×10^{20} cm^{-3}	**2.532**	**1.857**	**1.389**	**0.108**	**0.305**	**0.116**
$Zn_{0.82}Co_{0.18}O$: d = 396 nm, N_{Co}^{cal} = 6.392 × 10^{21} cm^{-3}, N_{Co}^{exp} = 3.327 × 10^{20} cm^{-3}, $\Sigma f_{i \to j}$ = 0.268						
Refractive index	**2.180**	**2.161**	**2.146**	**2.081**	**2.078**	**2.075**
$f_{i \to j}$, ×10^{-3}	**17.92**	**29.71**	**41.94**	**74.64**	**90.80**	**13.161**
N, ×10^{20} cm^{-3}	**0.931**	**1.173**	**0.845**	**0.205**	**0.027**	**0.146**
$Zn_{0.78}Co_{0.22}O$: d = 395 nm, N_{Co}^{cal} = 7.263 × 10^{21} cm^{-3}, N_{Co}^{exp} = 1.791 × 10^{20} cm^{-3}, $\Sigma f_{i \to j}$ = 0.417						
Refractive index	**2.182**	**2.164**	**2.149**	**2.085**	**2.082**	**2.078**
$f_{i \to j}$, ×10^{-3}	**22.72**	**36.66**	**41.92**	**106.3**	**111.3**	**98.643**
N, ×10^{20} cm^{-3}	**0.269**	**0.830**	**0.600**	**0.024**	**0.052**	**0.016**

1: 567 nm ($^4A_2(F) \to {}^2E(G)$); 2: 610 nm ($^4A_2(F) \to {}^4T_1(P)$); 3: 657 nm ($^4A_2(F) \to {}^2A_1(G)$); 4: 1297 nm ($^4A_2(F) \to {}^4T_1(F)$); 5: 1410 nm ($^4A_2(F) \to {}^4T_1(F)$); 6: 1647 nm ($^4A_2(F) \to {}^4T_1(F)$).

Table 5.
Level of absorbing sites N and oscillator strength f of Co^{2+} ions transition d-d.

film (d) as shown in **Figure 5**. The mathematical treatment of the coefficient of absorption is seen. It was possible to achieve a good fit for the multi-peak combination by optimizing the peak position and half-width of the Gaussian peaks.

At the bottom of **Figure 5**, the Gaussian peaks (dashed lines) while the solid line reflects the linear combination with a constant history of the multi-Gaussian peaks. **Table 4** shows the Gaussian peak position, field, width (eV) and height (α_{max}, cm^{-1}). The mathematical treatment of the absorption coefficient has shown that a series of overlapping bands consists of a large visible and near infrared spectral area. 0.75, ~0.86, ~0.96, ~1.87, ~22 are distinguished by six dominating bands.

Understanding the strengths of the oscillator $f_{i \to j}$ as determined from Eq. (7) The refractive index value of the intersubband transitions, i.e. at $\lambda_{i \to j}$ film, α_{max} and full width at half maximum W as defined by the Gaussian deconvolution of the absorption coefficient, enables the concentration of absorbing centers N. to be calculated from the formula of Smakula.

Table 5 displays the values obtained for the concentration of absorbing centers (N) and oscillator power (f) of the fingerprint of d-d transitions of Co^{2+} ions at the T_d symmetry sites.

For the investigated films, the amount of the oscillator intensity ($\Sigma f_{i \to j}$) from ground state $^4A_2(F)$ to all other states ranges from 0.006 to 0.417.

As mentioned above, the values of the direct optical band-gap is reduced from 3.26 to 3.00 eV. This significant band-gap reduction is due to enhanced Co^{2+} ions incorporation in the films as confirmed by the obtained concentration of absorbing centres.

In the deposition method by ultrasonic spray pyrolysis, the film growth is carried out by thermal decomposition of a precipitate at the substrate; This deposit results from the vaporization of the aerosol droplets. In this situation, the material that forms contains different types of impurities causing a disorder in the structure. In this case, the crystal lattice bounded by E_V and E_C may disappear. When the disorder becomes too high (eg with the appearance of dangling bonds or impurities in the material), the tails may encroach. We define the notion of Urbach parameter (E_{Urb}) to characterize this disorder. It is possible to estimate the existing disorder in

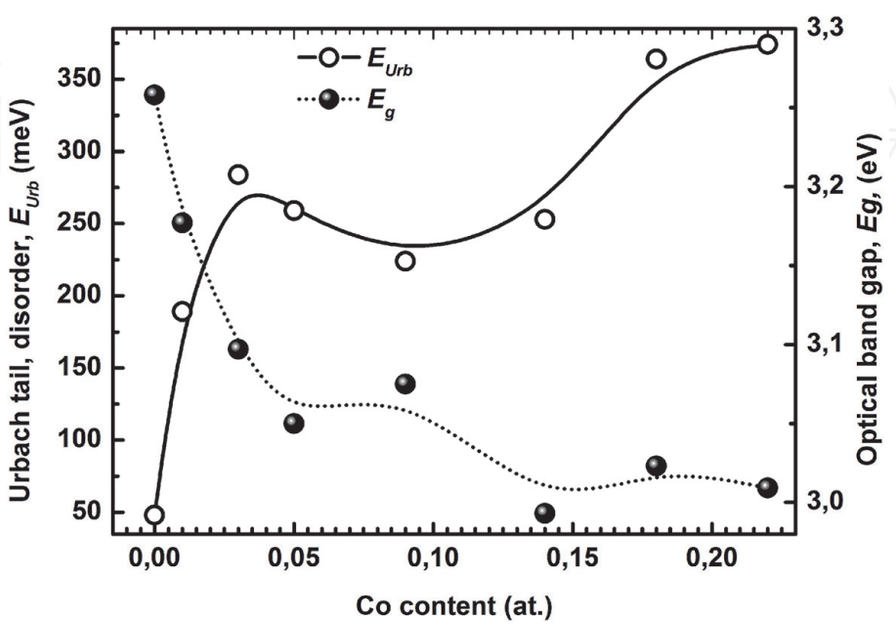

Figure 6.
Doping result and the variation of the bandgap and Urbach energy for different Co content.

the layers by studying the variations of the absorption coefficient. Indeed, the absorption coefficient can be expressed by the Equation [34]:

$$\alpha = \alpha_0 \exp\left(\frac{h\upsilon}{E_{Urb}}\right), \qquad h\upsilon \prec E_g$$

All our experimental results for the variation of the optical bandgap of the thin layers and disorders (Urbach energy of each sample is shown) as function of cobalt contents is shown in **Figure 6**. It is observed that the bandgap decreases with increasing cobalt content. The presence of high concentrations of localized states in the thin films is responsible for the reduction in the width of optical bandgap. Therefore, the addition of Co increases the concentration of localized states in the thin film leading to the decrease of the bandgap.

4. Conclusion

X-ray diffraction analysis using the Rietveld method shows that the as-deposited ZnO and $Zn_{1-x}Co_xO$ (x = 0.01–0.22) films are pure single wurtzite phase. The lattice parameter "*a*" increases with Co content while "*c*" seems to not much affected, thereby the volume of unit cell increases with increasing Co. However, the evolution of lattice parameters with Co content, is more complex than expected.

An optical model, which combines the Wemple-DiDomenico model, absorption coefficient of an electronic transition and Tauc-Urbach model, has been proposed to simulate the optical constants and thicknesses of Co doped ZnO films from normal incidence transmittance. The simulated transmission is found to be well matched to the measured transmission. The dispersion curves of the refractive index follow the model of the single oscillator. The dispersion parameters and the optical constants of the layers have been determined. The concentration of absorbing centres N_{Co} and oscillator strength f of d–d transition of Co^{2+} ions are also calculated from Smakula's formula.

The presence of high concentrations of localized states in the thin films is responsible for the reduction in the width of optical bandgap.

Acknowledgements

The authors would like to thank the National Project Research (PNR) and LASPI^{2}A Laboratory of Khenchela University (Algeria) for their financial support of this research project.

Author details

Sabrina Roguai[1*] and Abdelkader Djelloul[2]

1 LASPI[2]A Laboratory of Structures, Properties and Inter-Atomic Interactions, Abbes Laghrour University, Khenchela, Algeria

2 Science of Matter, Abbes Laghrour University, Khenchela, Algeria

*Address all correspondence to: rog.sabrina@yahoo.fr

IntechOpen

References

[1] Oktik S, Cost Low. non-vacuum tech niques for the preparation of thin/thick films for photovoltaic applications.Prog. Growth Charact. 1988; 17:171–240. doi : org/10.1016/0146-3535(88)90006-8

[2] Bouzid K., Djelloul A., Bouzid N, Bougdira J, Electrical resistivity and photoluminescence of zinc oxide films prepared by ultrasonic spray pyrolysis. Phys. Status Solid. A. 2009; 206:106–115. doi.org/10.1002/pssa.200824403

[3] Janotti A, Van de Walle Ch-G, Fundamentals of zinc oxide as asemiconductor. Rep. Prog. Phys. 2009; 72: 126501.

[4] Ellmer K, Klein A, Rech-(eds.) B, Transparent Conductive Zinc Oxide-Basics and Applications in Thin Film Solar Cells. Series: Springer Series in Materials Science.2008;104.

[5] Yang HM, Nie S. Preparation and characterization of Co-doped ZnO nanomaterials. Mater Chem Phys. 2009; 114: 279–282. doi: org/10.1016/j. matchemphys.2008.09.017

[6] Yang M., Guo ZX., Qiu KH, et al. Synthesis and characterization of Mn-doped ZnO column arrays. Appl Surf Sci. 2010;256: 4201–4205. doi :org/ 10.1016/j.apsusc.2010.01.125

[7] Saal H, Bredow T, Binnewies M. Band gap engineering of ZnO via doping with Manganese effect of Mn clustering. Phys Chem Chem Phys. 2009; 11: 3201–3209. doi :org/10.1039/B901596E

[8] Kumar GM, Ilanchezhiyan P, Kawakita J, et al. Magnetic and optical property studies on controlled low-temperature fabricated one dimensional Cr doped ZnO nanorods. Cryst Eng Commun. 2010; 12 :1887–1892. doi :org/ 10.1039/B924643F

[9] Fabbiyola S, Kennedy L-J, Aruldoss U, Bououdina M, Dakhel A-A, Judith Vijaya J, Synthesis of Co-doped ZnO nanoparticles via co-precipitation: structural, optical and magnetic properties. Powder. Technol. 2015; 286: 757–765. doi.org/10.1016/j.powtec. 2015.08.054

[10] Dietl T, Ohno H, Matsukura F, et al. Zener Model Description of Ferromagnetism in Zinc-Blende Magnetic Semiconductors. Science 2000 ;287 :1019–1022. doi: 10.1126/ science.287.5455.1019

[11] Wang YX, Ding X, Cheng Y, et al. Properties of Co-doped ZnO films prepared by electrochemical deposition. Cryst Res Technol. 2009;44(5):517–520. doi :org/10.1002/crat.200800466

[12] Song C, Zeng F, Geng KW, et al. The magnetic properties of Co-doped ZnO diluted magnetic insulator films prepared by direct current reactive magnetron co-sputtering. J Magn Magn Mater. 2007;309: 25–30.doi.org/ 10.1016/j. jmmm.2006.06.012

[13] Zukova A, Teiserskis A, Van Dijken S, et al. Giant moment and magnetic anisotropy in Co-doped ZnO films grown by pulse-injection metal organic chemical vapor deposition. Appl. Phys. Lett. 2006; 89:232503–232505. doi :org/10.1063/1.2399939

[14] Matsui H, Tabata H. Simultaneous control of growth mode and ferromagnetic ordering in Co-doped ZnO layers with Zn polarity. Phys Rev B. 2007; 75:014438–014447. doi : org/10.1103/PhysRevB.75.014438

[15] Sivagamasundari A, Pugaze R, Chandrasekar S, Rajagopan S, Kannan R, Absence of free carrier and paramagnetism in cobalt-doped ZnO nanoparticles synthesized at low

temperature using citrate sol-gel route. Appl. Nanosci. 2013;3: 383–388. DOI 10.1007/s13204-012-0146-0.

[16] Iqbal G, Faisal S, Khan S, Shams D-F, Nadhman A, Photo-inactivation and efflux pump inhibition of methicillin resistant *Staphylococcus aureus* using thiolated cobalt doped ZnO nanoparticles. Journal of Photochemistry & Photobiology. B: Biology.2019;192: 141–146. doi.org/10.1016/j.jphotobiol.2019.01.021

[17] Sindhu H-S, Kulkarni D-S, Choudhary R-J, Babu B-D, Rajendra B-V, Influence of cobalt doping on structure, optical and magnetic properties of spray pyrolysed nano structured ZnO films, Physica B: Physics of Condensed Matter.2019;578:18–26 doi.org/10.1016/j.physb.2019.07.034

[18] Ivill M, Pearton S-J, Rawal S, Leu L, Sadik P, Das R, Hebard A-F, Chisholm M, Budai John-D, and Norton David-P , Structure and magnetism of cobalt doped ZnO thin films. New Journal of Physics. 2008;10:065002

[19] Kohan A-F, Ceder G, Morgan D, Van de Walle C-G, First-principles of native point defects in ZnO. Physical Review B. 2000; 61: 15019. doi.org/10.1103/PhysRevB.61.15019

[20] Roguai S, Djelloul A., Nouveau C, et al. Structure, microstructure and determination of optical constants from transmittance data of co-doped $Zn_{0.90}Co_{0.05}M_{0.05}O$ (M = Al, Cu, Cd, Na) films. J. Alloys Compd.2014; 599:150–158 doi : org/10.1016/j.jallcom.2014.02.080

[21] Bouloudenine M, Viart N, Colis S, Kortus J, Dinia A. Antiferromagnetism in bulk $Zn_{1-x}Co_xO$ $Zn_{1-x}Co_xO$ magnetic semiconductors prepared by the coprécipitation technique. Appl. Phys. Lett.2005; 87: 052501. doi.org/10.1063/1.2001739

[22] Chen X-C, Zhou J-P, Wang H-Y, Xu P-S, Pan G-Q, Chin. Phys. B.2011; 20:9.

[23] Bao D, Gu H, Kuang A, Sol-gel-derived c-axis oriented ZnO thin films. Thin Solid Films. 1998;312,:37–39

[24] Benramache S, Benhaoua B, Influence of substrate temperature and Cobalt concentration on structural and optical properties of ZnO thin films prepared by Ultrasonic spray technique. Superlattices and Microstructures. 2012; 52: 807–815 doi.org/10.1016/j.spmi.2012.06.005.

[25] Wemple SH, DiDomenico M. Behavior of the Electronic Dielectric Constant in Covalent and Ionic Materials. Phys. Rev. B. 1971; 3: 1338–1351. DOI:https://doi.org/10.1103/PhysRevB.3.1338

[26] Tauc J, in: F. Abelès (Ed.), Optical Properties of Solids, North-Holland, Amsterdam, London.1972: 277–313.

[27] Davis EA, Mott NF. Conduction in non-crystalline systems V. Conductivity, optical absorption and photoconductivity in amorphous semiconductors. Philosophical Magazine. 1970; 22: 903–922. https://doi.org/10.1080/14786437008221061

[28] http://refractiveindex.info/?group=GLASSES&material=BK7.

[29] Ashour A, Kaid MA, El-Sayed NZ, Ibrahim AA. Physical properties of ZnO thin films deposited by spray pyrolysis technique. Appl. Surf. Sci.2006; 252: 7844–7848. https://doi.org/10.1016/j.apsusc.2005.09.048

[30] Lommens P, Smet PF, Donega CM, et al. Photoluminescence properties of Co^{2+}-doped ZnO nanocrystals.J. Lumin. 2006 ;118 : 245–250. doi : org/10.1016/j.jlumin.2005.08.020

[31] Pereira AS, Ankiewicz AO, Gehlhoff W, et al. Surface modification

of Co-doped ZnO nanocrystals and its effects on the magnetic properties. J Appl Phys. 2008 ;103: 07D140. doi: 10.1063/1.2833300

[32] Baklanov MR, Mogilnikov KP, Polovinkin VG, Dultsev FN. Determination of pore size distribution in thin films by ellipsometric porosimetry. J. Vac. Sci. Technol. B. 2000;18: 1385–1391. **https://doi.org/10.1116/1.591390**

[33] Smakula A. Über Erregung und Entfärbung lichtelektrisch leitender Alkalihalogenide. Zeitschrift für Physik. 1930; 59: 603–614.

[34] Pankove JI. Absorption Edge of Impure Gallium Arsenide. Phys. Rev. 1965;140: A 2059. DOI:https://doi.org/10.1103/PhysRev.140.A2059